This is the peer reviewed version of the following article: C.-Y. Huang, A. Bonasera, L. Hristov, Y. Garmshausen, B. M. Schmidt, D. Jacquemin, S. Hecht, *J. Am. Chem. Soc.* **2017**, *139* (42), 15205–15211, which has been published in final form at https://pubs.acs.org/doi/10.1021/jacs.7b08726. This article may be used for non-commercial purposes in accordance with ACS Publication Terms and Conditions for Self-Archiving. Supporting Information is available free of charge following the previous link.

N,N′-Disubstituted Indigos as Readily Available Red-Light Photoswitches with Tunable Thermal Half-Lives

Chung-Yang Huang, Aurelio Bonasera, Lachezar Hristov, Yves Garmshausen, Bernd M. Schmidt, Denis Jacquemin* and Stefan Hecht*

Abstract

Some rare indigo derivatives have been known for a long time to be photochromic upon irradiation with red light, which should be advantageous for many applications. However, the absence of strategies to tune their thermal half-lives by modular molecular design as well as the lack of proper synthetic methods to prepare a variety of such molecules from the parent indigo dye have so far precluded their use. In this work, several synthetic protocols for *N*-functionalization have been developed, and a variety of *N*-alkyl and *N*-aryl indigo derivatives have been prepared. By installation of electron-withdrawing substituents on the *N*-aryl moieties, the thermal stability of the *Z*-isomers could be enhanced while maintaining the advantageous photoswitching properties upon irradiation with red light (660 nm LED). Both experimental data and computational results suggest that the ability to tune thermal stability without affecting the dyes' absorption maxima originates from the twisted geometry of the *N*-aryl groups. The new indigo photoswitches reported are expected to have a large impact on the development of optical methods and applications in both life and material sciences.

Introduction

In recent years the field of photochromism research has witnessed exciting developments, and photoswitchable molecules have been broadly applied in various disciplines of science. In particular in the context of biomedical applications, photoswitches have become a key tool to remotely and noninvasively regulate processes (1) in vivo, for example, associated with photopharmacology, (2) super-resolution fluorescence imaging, (3) and optochemical genetics. (4) To successfully implement photoswitches in biological systems, they have to meet three important criteria: First, the molecules should be able to undergo efficient photoisomerization upon irradiation with red or infrared light due to its superior ability to penetrate

tissues ("biological window"). (5) Second, the two isomers should possess significantly different structures to maximize the light-induced activity modulation. Third, the thermal half-life of the metastable, ideally biologically active, isomer should be tunable to adjust its in vivo residence time according to circulation or other parameters of interest.

To date, azobenzenes have been the most promising candidates due to their significant structural changes as a result of the *E*–*Z* isomerization as well as their established photochemistry and the straightforward synthesis. (6) Recent efforts by multiple groups have led to the development of novel azo compounds addressable by visible light, (7) clearly improving their applicability. Despite the significant progress made, these molecules are oftentimes not red-shifted enough for biological applications, even after delicate modifications of the azo framework. Thus, it is (still) desirable to develop even more red-shifted photoswitches. To our surprise, indigo, one of the most ancient dyes known in human history, has been left out in this recent wave of developments, although its photoisomerization under the influence of red light has been described more than half a century ago. (8) This is presumably due to the fact that the parent, unsubstituted indigo does not undergo photoinduced *E*–*Z* isomerization because of its dominating and very efficient deactivation via excited state intramolecular proton transfer. (9) In strong contrast, *N*,*N*′-disubstituted indigos, carrying no amide protons, are capable of undergoing efficient *E*–*Z* photoisomerization (Scheme 1). (8, 10-12)

Photoswitches based on indigos in principle offer several promising advantages. First and foremost, they could be prepared from highly abundant, low-cost materials. Due to their extended π-system and its inherent push–pull character, arising from coupling two charge-transfer halves in a so-called H-chromophore, (13) indigos intrinsically absorb in the red region of the spectrum, even without specific donor/acceptor derivatization. Importantly, *E*–*Z* isomerization confers larger structural changes, in particular with regard to substituents projected from the indigo N-atoms as compared to the commonly exploited azobenzene *para*-positions, thus rendering indigos superior steric switches. In addition, indigo photoswitches should presumably exhibit reasonably low toxicity as evidenced by their extensive use for centuries. Last but not least, indigos display negative photochromism, (14) providing a means to enhance penetration depth through the course of irradiation and therefore facilitating their application in pharmacology and bulk materials.

To date, symmetrical *N*,*N*′-diacyl, (10) *N*,*N*′-dimethyl, (11) and *N*,*N*′-di(*tert*-butyloxycarbonyl) (12) indigos are among the only reported photoswitches in this family. Their absorption maxima (λ_{max}) range from 530 nm all the way to 670 nm, which is strongly red-shifted when compared to conventional *E*–*Z* photoswitches, such as stilbenes and azobenzenes. (7a) However, these compounds suffer from either poor hydrolytic stability or lack of direct functionalization, and more importantly, molecular design rules allowing to rationally tune their thermal half-lives remain elusive. Herein, we report a series of symmetrical and nonsymmetrical *N*-alkyl- and *N*-aryl-substituted indigos, which allow for systematic modulation of their thermal half-lives by direct structural modification of the parent indigo while maintaining its advantageous red-shifted absorption (Scheme 1).

Results and discussion

The initial hurdle that we had to overcome was the lack of synthetic methods known to install *N*-substituents on the parent indigo. According to scattered reports in the literature, *N*-alkylation and *N*-arylation often require harsh conditions and result in complex mixtures and low yields. We tried to circumvent this problem by identifying appropriate functionalization reagents that would provide enhanced reactivity yet under milder conditions. To our delight, by using a weak base and activated electrophiles, such as benzyl bromide or α-bromoacetate, double *N*-alkylation of indigo can be achieved at room temperature (Scheme 2, method A). Furthermore, we developed two sets of complementary conditions that allow for double *N*-arylation (15) of indigo under mild conditions. For installing electron-rich or electron-neutral aryl substituents, it was found that Chan-Lam coupling is the most suitable (Scheme 2, method B), (16) while in the case of electron-deficient aryl groups, Cu-catalyzed cross-coupling reaction with aryliodonium salts was applied (Scheme 2, method C). (17) Interestingly, both methods are extremely selective toward double *N*,*N*′-arylation, and only minor amounts of mono-*N*-arylated products were observed. However, to gain full synthetic flexibility for functionalizing indigos, the ability to prepare nonsymmetrical compounds is also critical. In this context, a Goldberg–Ullmann reaction proved useful as it reliably provides the mono-*N*-arylated indigos (Scheme 2, method D), (18) which subsequently can be alkylated or arylated using the previously described methods A–C to obtain indigos with two different *N*,*N*′-substituents. Although these reactions have not yet been fully optimized, they serve as rapid and straightforward entries into symmetrical and nonsymmetrical *N*,*N*′-disubstituted indigos from the abundant and inexpensive parent indigo dye. All of the prepared compounds were obtained as dark blue or green solids, and, unlike their parent indigo precursor, they are readily soluble in most organic solvents, simplifying purification, characterization, and further processing.

Our initial studies focused on compounds in series I, i.e., *N*,*N*′-dialkylindigos (Table 1). In accordance with the literature, (11) *N*,*N*′-dimethylindigo **2** and *N*,*N*′-dibenzylindigo **3** are among the most red-shifted compounds examined in this study, whereas in the case of *N*,*N*′-di(benzyloxycarbonyl-methyl)indigo **4** (Figure 1), the presence of electron-withdrawing ester groups causes a slight blue shift by 20 nm. Upon irradiation with a red LED (660 nm, 20 nm full width at half-maximum (fwhm)), the intensity of the long-wavelength absorption band decreased, and a shoulder below 600 nm started to rise. When the light was turned off, **2** and **3** returned to their initial state immediately, whereas **4** showed a slower recovery with a thermal half-life ($t_{1/2}$) of 2.8 min at room temperature (see Figure 1c, d for a representative photochemical forward and thermal back isomerization). The fact that these indigo photoswitches exhibit negative photochromism allowed us to obtain the composition of the photostationary state (PSS) and the absorption spectrum of the pure *Z*-isomer directly from the *E* and PSS spectra (see Section III of the Supporting Information). Applying this methodology, we found that the absorption maxima of *E*-**4** and *Z*-**4** are well separated ($\Delta\lambda_{max}$ = 62 nm).

Next, we turned our attention to nonsymmetrical indigos substituted with one aryl and one alkyl group each. First, we compared series II, in which the aryl moiety (4-trifluoromethylphenyl) was kept constant and the

alkyl group was varied (Table 2). Similar to what we observed in *N*,*N*′-dialkylindigos, the presence of the electron-withdrawing ester group in **6** causes a slight blue shift and an increased thermal half-life of the *Z*-isomer. However, in compound **7**, where the *tert*-butyloxycarbonyl group is attached directly to the indigo *N*-atom, a much larger blue shift as well as a much longer thermal half-life was observed. These findings are in line with the behavior of *N*,*N*′-diacyl (10) and *N*,*N*′-di(*tert*-butyloxy-carbonyl) (12) indigos, in which the electron-withdrawing carbonyl-based *N*-substituents result in thermally much more stable *Z*-isomers and yet inevitable significantly blue-shifted absorption spectra, rendering them no longer suitable for operation using red light. In order to overcome this problem, we subsequently decided to explore substituent effects on the *N*-aryl rings.

In series III we therefore fixed the CH_2CO_2tBu as the alkyl group and studied the electronic effect of *para*-substituents on the aryl ring (Table 3). We found that the nature of the substituents does not have a large influence on the absorption maximum of the *E*-isomer, which for the entire series remains in the red domain ($623 \leq \lambda_{max} \leq 633$ nm). Introduction of electron-withdrawing substituent leads to an increased spectral separation of the absorption maxima of *E*- and *Z*-isomers. In addition, we observed a sixfold increase in thermal half-life when changing from an electron-donating methoxy (**8**) to an electron-withdrawing cyano group (**10**). Thus, in acceptor-substituted indigo **10**, both enhanced spectral separation and thermal lifetime lead to a much larger *Z*-content in the PSS as compared to indigo **8**. More importantly, this finding demonstrates that the thermal half-life of indigo photoswitches can indeed be tuned independently from their absorption spectra by proper structural modification and encouraged us to pursue *N*,*N*′-arylated indigo derivatives.

Utilizing the synthetic methods developed by us for indigo *N*-arylation, we finally prepared two series of symmetrically as well as nonsymmetrically substituted *N*,*N*′-diaryl indigos (series IV and V). To our surprise, NMR analysis for these compounds revealed that they all exist as a mixture of *E*- and *Z*-isomers. Typically, we observe an *E*/*Z* ratio between 2:1 and 3:1 in CD_2Cl_2 (see Section VIII of the Supporting Information). The existence of such mixtures in the dark state implies that the stability of both isomers is rather comparable and that the separating barrier allows for thermal isomerization (in both directions) at room temperature. DFT-computed relative free energies of the two isomers (see Table S1 in the Supporting Information) confirm that the bis-arylated indigos exhibit negligible ground-state energy differences between the two isomers. Indeed, we determined free energy differences smaller than 1 kcal/mol between the Z- and *E*-isomers of **11**–**18**, a value which is within the typical DFT error bar, indicating nearly isoenergetic structures. A possible explanation involves attractive π–π interactions between the two aryl moieties in the *Z*-isomer on the one hand and repulsive interactions between the aryl moiety and the indigo carbonyl group in the *E*-isomer on the other hand. Both of these interactions are plausible by comparing the molecular structures (Figure 2 for *E*-**12** vs *Z*-**12**), obtained by single-crystal X-ray diffraction and quantum chemical calculation (see Table S2 of the Supporting Information).

Irradiating these *N*,*N*′-diaryl indigos with a red LED (660 nm, fwhm = 20 nm) led to a different *E*/*Z* ratio in the PSS. Based on ^{19}F-NMR spectroscopy, compound **14** went from a dark mixture containing 26% *Z*-isomer

to a solution containing 81% *Z*-isomer in the PSS at room temperature, and when this sample was left in the dark, it returned to the initial *E/Z* mixture (Figure 3 and Supporting Information). Initial cycling experiments with compound **12** indicated a robust switching process without noticeable fatigue (see Section XI in the Supporting Information).

Subsequently, we analyzed the kinetics of the thermal back reaction. (19) To describe the time required for returning from the PSS to the thermodynamic equilibrium in the dark, we introduce here the term "equilibration thermal half-life $t(\mathrm{eq})_{1/2}$". Following the recovery of absorbance at 620 nm, $t(\mathrm{eq})_{1/2}$ was obtained for each compound (Table 4). A clear trend of how the substitution pattern influences $t(\mathrm{eq})_{1/2}$ was observed as increasingly electron-withdrawing groups result in longer $t(\mathrm{eq})_{1/2}$, spanning a range from 58 s for OMe (**11**) to 408 min for NO_2 (**16**). Importantly, this dramatic difference in the rate of thermal recovery is accompanied by negligible changes in the absorption maxima (λ_{max}) of the molecules, which remain red-shifted regardless of their substitution, and thus a red LED (660 nm, fwhm = 20 nm) was utilized in all cases to successfully induce the photoisomerization.

The observed correlation between the *N*-aryl substituents and thermal half-lives led us to further investigate the process of thermal relaxation. Comparing the compounds from series III through V, it appears that in general *N*-arylation seems to stabilize the *Z*-isomer relative to the *E*-isomer while at the same time the transition state (TS) does not seem to be affected, leading to a net increase of the thermal barrier. This is reflected by the analysis of our kinetic data that shows a linear correlation between the rate constants for thermal equilibration and Hammett's substituent parameters (20) for both series III and IV (Figure 4 and Section VIII of the Supporting Information). In both cases the slope is clearly negative, indicating that electron-deficient aryl moieties, in particular when attached to both indigo *N*-atoms, slow down thermal return from the photostationary to the dark state.

We performed broken-symmetry density functional theory (BS-DFT) calculations aiming to determine and characterize the TS for all dyes of series IV and V (see Section XII of the Supporting Information). The obtained TS geometries exhibit a dihedral angle close to 90° between the two halves of the molecules, and the associated imaginary frequency is close to $50i$ cm^{-1} (Figure 5b). Gratifyingly, the correlation found between our experimental and theoretical data is remarkable (R^2 = 0.97, Figure 5a), confirming the accuracy of our computational model and thus providing a solid foundation and encouraging prospect to design indigo derivatives with improved thermal stability. More detailed analysis of the TS (see Section XII of the Supporting Information) indicates that the largest spin density of the unpaired electron on each side is located on each of the neighboring bridging carbon atoms (ca. 0.5 e) whereas the spin density borne by the oxygen atoms is smaller (ca. 0.3 e). In addition, the Mulliken electronic charges borne by the oxygen atoms are only marginally larger in the TS (ca. −0.6 e) as compared to the *Z*- and *E*-isomers (ca. −0.5 e). These findings are in agreement with a predominant biradical character of the TS. (10h)

We have also characterized the derivatives of series IV and V using time-dependent DFT. The theoretically predicted absorption maxima (see Table S3 of the Supporting Information) are well in line with the experimentally observed values for both *Z*- and *E*-isomers. As expected, the absorption maxima of all

compounds and isomers are related to the lowest excited state, which can be assigned to a HOMO → LUMO transition. These frontier orbitals are centered on the H-chromophore of the indigo core (Figure 5c, d), and the aryl substituents contribute only little, explaining the relatively small variations of the absorption spectra (see Table 4). This decoupling of the aryl units is due to their almost perpendicular orientation relative to the plane of the indigo. Consequently, these groups can influence the central chromophore only via an inductive effect, in contrast to the carbonyl-based *N*-substituents, such as in **7**, where resonance effects predominate, resulting in more stable *Z*-isomers yet significantly blue-shifted absorption spectra of the *E*-isomers.

An important merit of indigo photoswitches is their superior ability to change the distance between two functional motifs by light. A closer examination of both the DFT-optimized *E*- and *Z*-isomers of indigos **4**, **6**, and **12** revealed that during the course of photoisomerization a change of distance between the two substituents of 2.7, 3.8, and 3.5 Å, respectively, can be achieved (see Table S2 in the Supporting Information), which is, for the arylated indigos, slightly superior to the ca. 3 Å change that is generally exerted by azobenzenes. This finding demonstrates the potential of indigos to serve as superior steric switch. Furthermore, DFT calculations indicate that *E*–*Z* photoisomerization is able to induce significant changes in dipole moment of up to 7 D between the two isomers (see Table S1 in the Supporting Information).

Conclusion

In conclusion, we have revisited the classical indigo chromophore motif and developed a strategy to tune the thermal stability of the *Z*-isomers independently from the advantageous optical spectra. The introduction of electron-withdrawing *N*-aryl substituents has proven key to achieve sufficiently long thermal half-lives of the *Z*-isomers, which are attractive for biomedical applications, while maintaining the compounds' absorption in the red and hence photoisomerization ability with 660 nm light. In contrast to previously reported amide-containing indigos, (10, 12) the new indigo derivatives display excellent hydrolytic stability in aqueous solutions containing acetonitrile to facilitate solubility. Using a combined experimental and theoretical approach, we have gained general insight into the factors determining the thermal stability of the indigo isomers and their electronic and geometrical structure, encoding both their optical properties and activity differences. The latter are expected to be significant due to large geometry changes during photoisomerization and promise that indigos might indeed perform as superior steric photoswitches. Thus, our work introduces an exciting new generation of indigo derivatives, which are readily derived from one of the cheapest and most abundant dyes on the planet and which should greatly expand the tool box available to researchers, pursuing to exploit photoswitches in future life and material science applications.

Acknowledgements

This work is dedicated to the memory of Lachezar Hristov. The authors thank Dr. Benjamin Koeppe for initial discussions and Dr. Andre Dallmann for help with NMR analysis. C.-Y.H. and B.M.S. are indebted to the Alexander von Humboldt Foundation for providing postdoctoral fellowships. L.H. was supported by a Fulbright predoctoral fellowship. Generous support by the European Research Council (ERC via ERC-2012-STG_308117 "Light4Function") and the German Research Foundation (DFG via SFB951, project A3) is gratefully acknowledged. This work used the computational facilities of the CCIPL center installed in Nantes.

References

(1) Szymański, W.; Beierle, J. M.; Kistemaker, H. A. V.; Velema, W. A.; Feringa, B. L. *Chem. Rev.* **2013**, *113*, 6114– 6178.

(2) (a) Velema, W. A.; Szymański, W.; Feringa, B. L. *J. Am. Chem. Soc.* **2014**, *136*, 2178– 2191; (b) Broichhagen, J.; Frank, J. A.; Trauner, D. *Acc. Chem. Res.* **2015**, *48*, 1947– 1960; (c) Lerch, M. M.; Hansen, M. J.; van Dam, G. M.; Szymański, W.; Feringa, B. L. *Angew. Chem., Int. Ed.* **2016**, *55*, 10978– 10999.

(3) Heilemann, M.; Dedecker, P.; Hofkens, J.; Sauer, M. *Laser Photonics Rev.* **2009**, *3*, 180– 202.

(4) Fehrentz, T.; Schönberger, M.; Trauner, D. *Angew. Chem., Int. Ed.* **2011**, *50*, 12156– 12182.

(5) Pansare, V. J.; Hejazi, S.; Faenza, W. J.; Prud'homme, R. K. *Chem. Mater.* **2012**, *24*, 812– 827.

(6) (a) Beharry, A. A.; Woolley, G. A. Chem. Soc. Rev. **2011**, 40, 4422– 4437; (b) Mart, R. J.; Allemann, R. K. Chem. Commun. **2016**, 52, 12262– 12277.

(7) An overview is given in: (a) Bléger, D.; Hecht, S. *Angew. Chem., Int. Ed.* **2015**, *54*, 11338– 11349. Examples include: (b) Siewertsen, R.; Neumann, H.; Buchheim-Stehn, B.; Herges, R.; Nather, C.; Renth, F.; Temps, F. *J. Am. Chem. Soc.* **2009**, *131*, 15594– 15595; (c) Beharry, A. A.; Sadovski, O.; Woolley, G. A. *J. Am. Chem. Soc.* **2011**, *133*, 19684– 19687; (d) Samanta, S.; Qin, C.; Lough, A. J.; Woolley, G. A. *Angew. Chem., Int. Ed.* **2012**, *51*, 6452– 6455; (e) Yang, Y.; Hughes, R. P.; Aprahamian, I. *J. Am. Chem. Soc.* **2012**, *134*, 15221– 15224; (f) Bléger, D.; Schwarz, J.; Brouwer, A. M.; Hecht, S. *J. Am. Chem. Soc.* **2012**, *134*, 20597– 20600; (g) Samanta, S.; Beharry, A. A.; Sadovski, O.; McCormick, T. M.; Babalhavaeji, A.; Tropepe, V.; Woolley, G. A. *J. Am. Chem. Soc.* **2013**, *135*, 9777– 9784; (h) Bushuyev, O. S.; Tomberg, A.; Friščić, T.; Barrett, C. J. *J. Am. Chem. Soc.* **2013**, *135*, 12556– 12559; (i) Knie, C.; Utecht, M.; Zhao, F.; Kulla, H.; Kovalenko, S.; Brouwer, A. M.; Saalfrank, P.; Hecht, S.; Bléger, D. *Chem. - Eur. J.* **2014**, *20*, 16492– 16501; (j) Weston, C. E.; Richardson, R. D.; Haycock, P. R.; White, A. J. P.; Fuchter, M. J. *J. Am. Chem. Soc.* **2014**, *136*, 11878– 11881; (k) Hansen, M. J.; Lerch, M. M.; Szymanski, W.; Feringa, B. L. *Angew. Chem., Int. Ed.* **2016**, *55*, 13514– 13518; (l) Stricker, L.; Fritz, E.-C.; Peterlechner, M.; Doltsinis, N. L.; Ravoo, B. J. *J. Am. Chem. Soc.* **2016**, *138*, 4547– 4554; (m) Calbo, J.; Weston,

C. E.; White, A. J. P.; Rzepa, H. S.; Contreras-García, J.; Fuchter, M. J. *J. Am. Chem. Soc.* **2017**, *139*, 1261– 1274.

(8) Wyman, G. M. *Chem. Rev.* **1955**, *55*, 625– 657.

(9) Pina, J.; Sarmento, D.; Accoto, M.; Gentili, P. L.; Vaccaro, L.; Galvão, A.; de Melo, J. S. S. *J. Phys. Chem. B* **2017**, *121*, 2308– 2318 and references therein.

(10) (a) Brode, W. R.; Pearson, E. G.; Wyman, G. M. *J. Am. Chem. Soc.* **1954**, *76*, 1034– 1036; (b) Wyman, G. M.; Zenhäusern, A. F. *J. Org. Chem.* **1965**, *30*, 2348– 2352; (c) Giuliano, C. R.; Hess, L. D.; Margerum, J. D. *J. Am. Chem. Soc.* **1968**, *90*, 587– 594; (d) Omote, Y.; Imada, S.; Matsuzaki, R.; Fujiki, K.; Nishio, T.; Kashima, C. *Bull. Chem. Soc. Jpn.* **1979**, *52*, 3397– 3399; (e) Setsune, J.-I.; Wakemoto, H.; Matsukawa, K.; Ishihara, S.-I.; Yamamoto, R.-I.; Kitao, T. *J. Chem. Soc., Chem. Commun.* **1982**, 1022– 1023; (f) Omote, Y.; Tomotake, A.; Aoyama, H.; Nishio, T.; Kashima, C. *Bull. Chem. Soc. Jpn.* **1984**, *57*, 470– 472; (g) Pouliquen, J.; Wintgens, V.; Toscano, V.; Jaafar, B. B.; Tripathi, S.; Kossanyi, J.; Valat, P. *Can. J. Chem.* **1984**, *62*, 2478– 2486; (h) Sueishi, Y.; Ohtani, K.; Nishimura, N. *Bull. Chem. Soc. Jpn.* **1985**, *58*, 810– 814; (i) Görner, H.; Pouliquen, J.; Kossanyi, J. *Can. J. Chem.* **1987**, *65*, 708– 717.

(11) (a) Weinstein, J.; Wyman, G. M. *J. Am. Chem. Soc.* **1956**, *78*, 4007– 4010; (b) Miehe, G.; Süsse, P.; Kupcik, V.; Egert, E.; Nieger, M.; Kunz, G.; Gerke, R.; Knieriem, B.; Niemeyer, M.; Lüttke, W. *Angew. Chem., Int. Ed.* **1991**, *30*, 964– 967.

(12) (a) Głowacki, E. D.; Voss, G.; Demirak, K.; Havlicek, M.; Sünger, N.; Okur, A. C.; Monkowius, U.; Gąsiorowski, J.; Leonat, L.; Sariciftci, N. S. *Chem. Commun.* **2013**, *49*, 6063– 6065; (b) Farka, D.; Scharber, M.; Głowacki, E. D.; Sariciftci, N. S. *J. Phys. Chem. A* **2015**, *119*, 3563– 3568.

(13) (a) Klessinger, M.; Lüttke, W. *Tetrahedron* **1963**, *19*, 315– 335; (b) Dähne, S.; Leupold, D. *Angew. Chem., Int. Ed.* **1966**, *5*, 984– 993.

(14) Bouas-Laurent, H.; Dürr, H. *Pure Appl. Chem.* **2001**, *73*, 639– 665.

(15) Matsumoto, Y.; Tanaka, H. *Heterocycles* **2003**, *60*, 1805– 1810.

(16) Qiao, J. X.; Lam, P. Y. S. *Synthesis* **2011**, *6*, 829– 856.

(17) Yoshimura, A.; Zhdankin, V. V. *Chem. Rev.* **2016**, *116*, 3328– 3435

(18) Kim, I. K.; Li, X.; Ullah, M.; Shaw, P. E.; Wawrzinek, R.; Namdas, E. B.; Lo, S.-C. *Adv. Mater.* **2015**, *27*, 6390– 6395

(19) (a) Delbaere, S.; Vermeersch, G.; Micheau, J.-C. *J. Photochem. Photobiol., C* **2011**, *12*, 74– 105; (b) Hemmer, J. R.; Poelma, S. O.; Treat, N.; Page, Z. A.; Dolinski, N. D.; Diaz, Y. J.; Tomlinson, W.; Clark, K. D.; Hooper, J. P.; Hawker, C.; Read de Alaniz, J. *J. Am. Chem. Soc.* **2016**, *138*, 13960– 13966.

(20) (a) Hammett, L. P. *J. Am. Chem. Soc.* **1937**, *59*, 96– 103. A review is given in: (b) Hansch, C.; Leo, A.; Taft, R. W. *Chem. Rev.* **1991**, *91*, 165– 195.

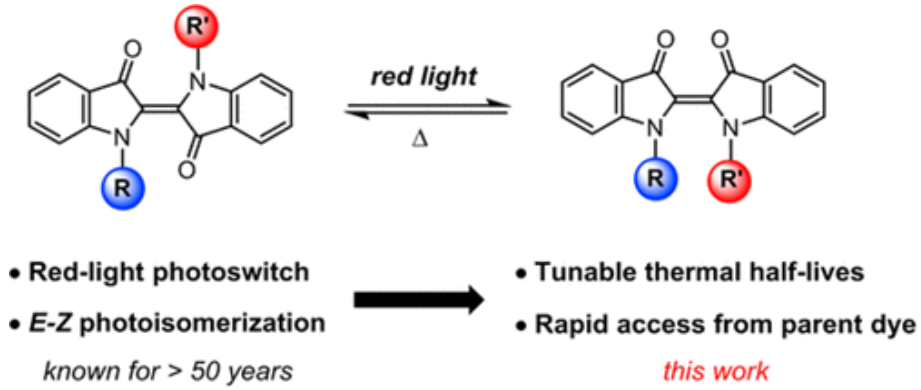

Scheme 1. Photoswitchable *N*,*N*′-Disubstituted Indigos

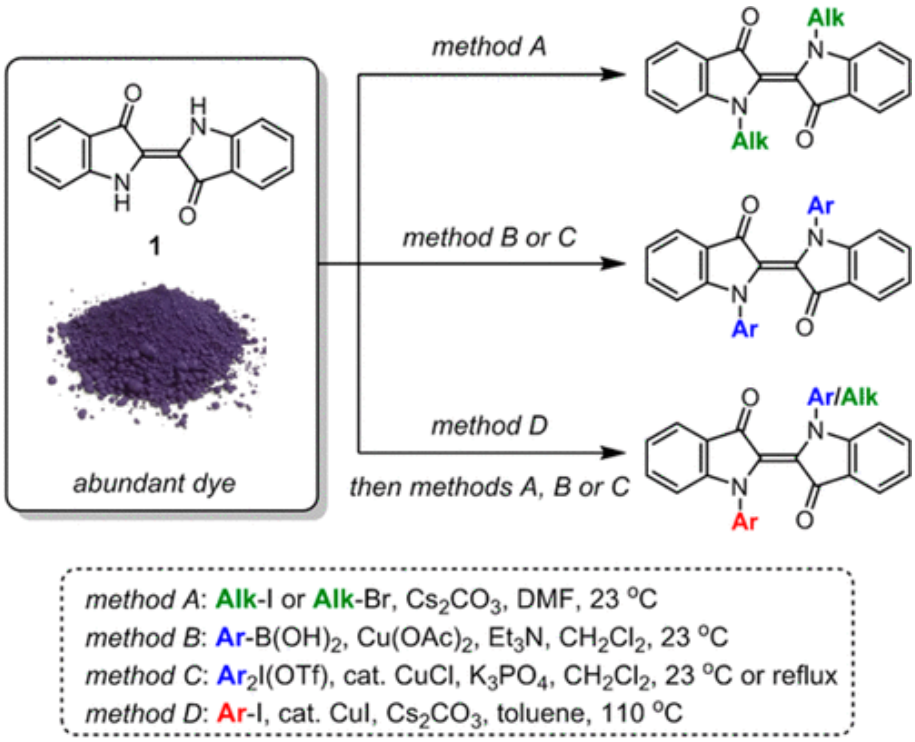

Scheme 2. Approaches for Indigo Functionalization

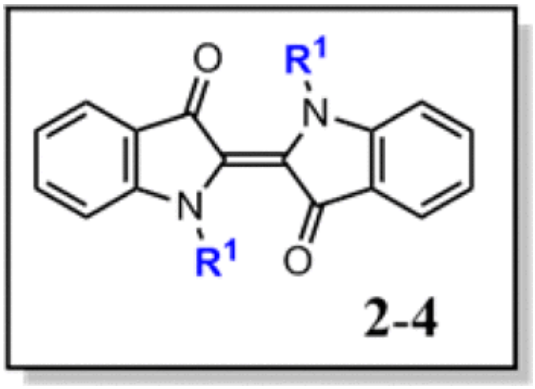

	series I: R1 =		
	Me (2)	**Bn (3)**	**CH2CO2*t*Bu (4)**
λmax, *E* (nm)	641	648	623
λmax, *Z* (nm)	n.a. [a]	n.a. [a]	561
ε*E* (M–1 cm–1)	16700	10800	15700
*t*1/2	<5 s	<5 s	2.8 min
Z-content PSS	n.a. [a]	n.a. [a]	77%
ϕ*E*–*Z* (578 nm)	n.a. [a]	n.a. [a]	0.06 [b]
ϕ*Z*–*E* (578 nm)	n.a. [a]	n.a. [a]	0.60 [b]

[a] Not available due to extremely short lifetime of *Z*-isomer.

[b] Determined at 25 °C.

Table 1. Photochemical Properties of Series I in CH_3CN

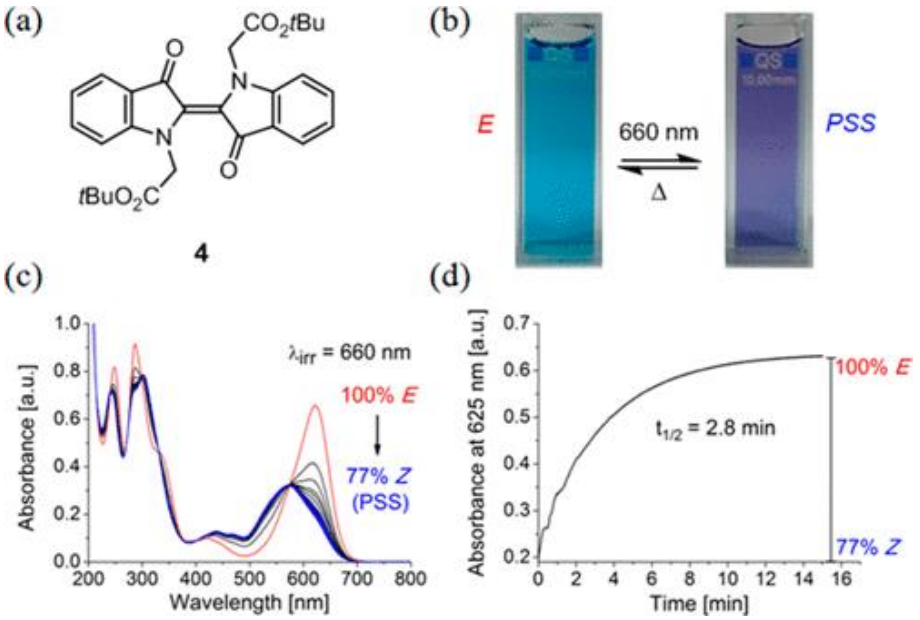

Figure 1. Photochromic and thermal behavior of indigo 4. (a) Chemical structure. (b) Photographs of *E*-4 and PSS-4 solutions in CH_3CN. (c) Evolution of the PSS upon irradiation with 660 nm LED with spectra taken every 30 s over 10 min at 25 °C (4.2×10^{-5} M in CH_3CN). (d) Thermal recovery at 25 °C monitored by absorbance at 625 nm in the dark.

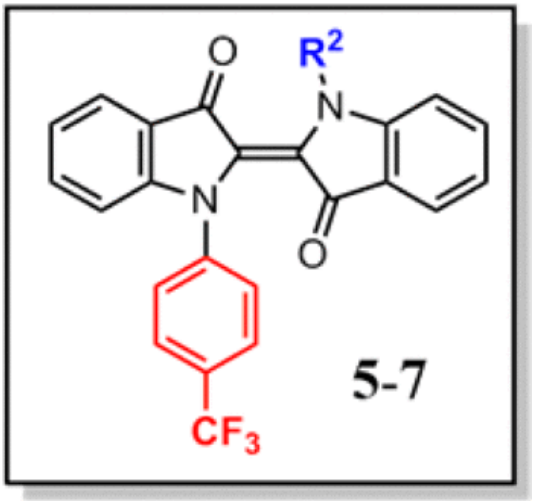

	series II: R2 =		
	Me (5)	**CH2CO2*t*Bu (6)**	**Boc (7)**
λmax, *E* (nm)	635	622	584
λmax, *Z* (nm)	595	572	525
ε*E* (M–1 cm–1)	13000	13200	9900
*t*1/2	57 s	3.5 min	193 min
Z-content PSS	38%	56%	80%
ϕ*E*–*Z* [a]	0.04	0.03	0.12
ϕ*Z*–*E* [a]	0.04	0.03	0.05

[a] Determined at −5 °C and 578 nm (see Supporting Information for full details).

Table 2. Photochemical Properties of Series II in CH_3CN

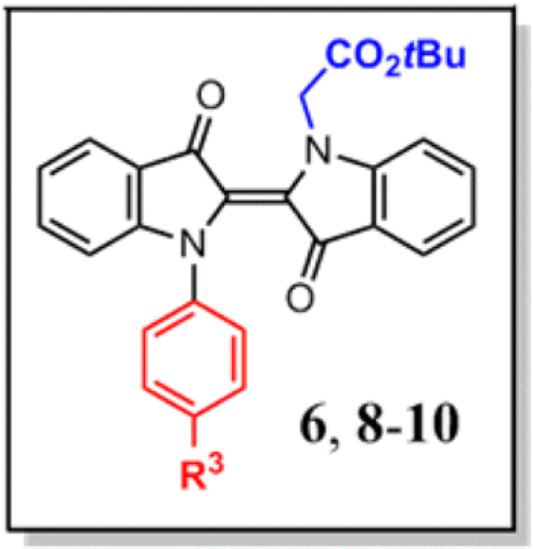

	series III: R3 =			
	OMe (8)	**H (9)**	**CF3 (6)**	**CN (10)**
λmax, *E* (nm)	633	629	622	623
λmax, *Z* (nm)	593	578	572	567
εE (M–1 cm–1)	13500	11900	13200	9800
*t*1/2	59 s	1.9 min	3.5 min	5.8 min
Z-content PSS	11%	62%	56%	71%
ϕ*E*–*Z* [a]	0.05	0.01	0.03	0.05
ϕ*Z*–*E* [a]	0.04	0.10	0.03	0.04

[a] Determined at −5 °C and 578 nm (see Supporting Information for full details).

Table 3. Photochemical Properties of Series II in CH_3CN

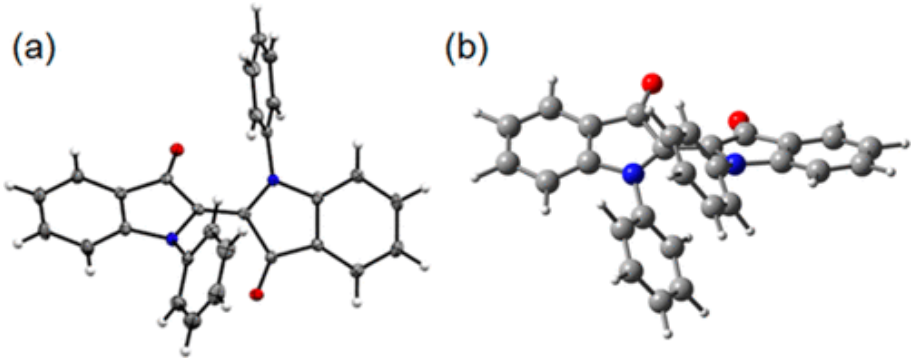

Figure 2. (a) X-ray structure of *E*-**12** (50% probability ellipsoids). (b) DFT-computed structure of *Z*-**12** (for details see Section XII of the Supporting Information).

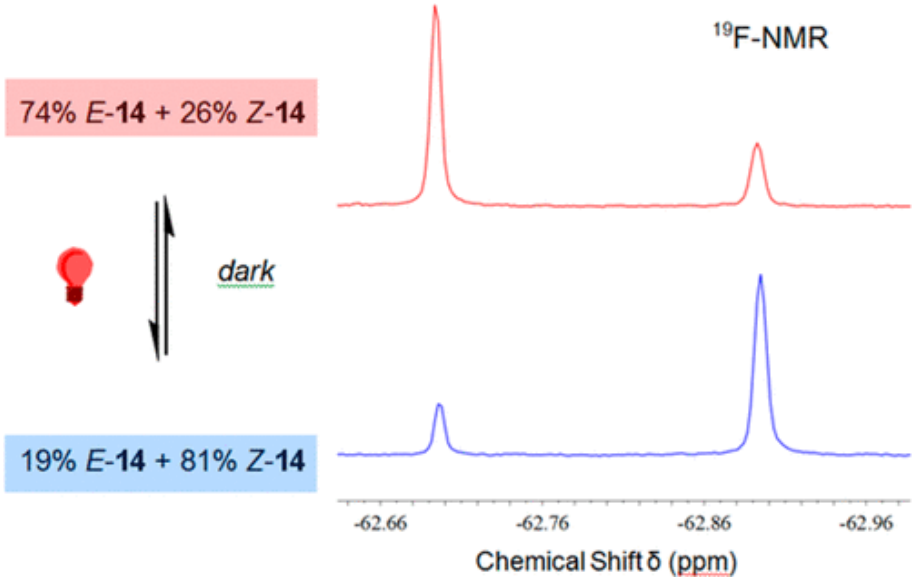

Figure 3. ^{19}F-NMR spectra of dark vs irradiated indigo **14**. Thermally equilibrated *E*/*Z* mixture of **14** (ca. 10^{-4} M in CD_3CN) in the dark (top) and after irradiation with 660 nm LED for 3 h at 25 °C (bottom). The initial spectrum (top) is recovered in the dark overnight (see Supporting Information for ^{1}H- and 2D NMR spectra).

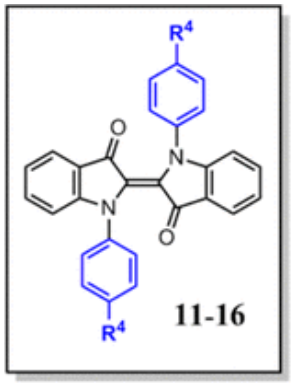

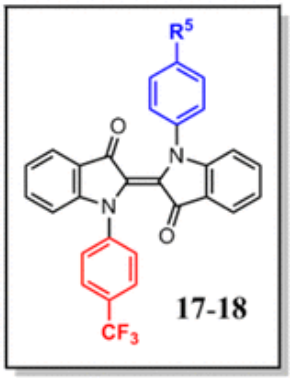

	series IV: R4 =						series V: R5 =	
	OMe (11)	**H (12)**	**F (13)**	**CF3 (14)**	**CN (15)**	**NO2 (16)**	**OMe (17)**	**F (18)**
λmax, *E* (nm)	645	635	630	621	619	620	632	624
λmax, *Z* (nm)	599	594	584	577	568	577	590	582
Z-content dark	33%	24%	34%	27%	25%	12%	39%	33%
t(eq)1/2	58 s	3.1 min	7.9 min	81 min	187 min	408 min	13 min	19 min
Z-content PSS	52%	64%	71%	83%	80%	82%	67%	76%
ϕ*E*–*Z* [a]	n.d. [b]	n.d. [b]	0.13	0.06	0.06	0.07	0.36	0.15
ϕ*Z*–*E* [a]	n.d. [b]	n.d. [b]	0.08	0.04	0.03	0.04	0.08	0.08

[a] Determined at 25 °C and 578 nm (except for **17** at 546 nm; see Supporting Information for full details).

[b] Not determined due to short lifetime of Z-isomer.

Table 4. Photochemical Properties of Series IV and V in CH_3CN

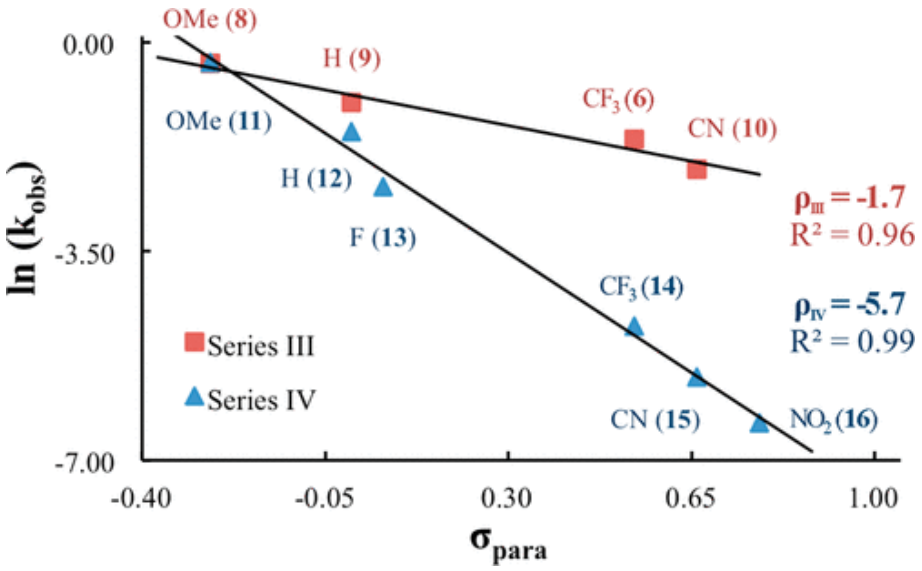

Figure 4. Hammett plots of the rate of thermal equilibration (from the PSS to the dark state) for indigo series III and IV.

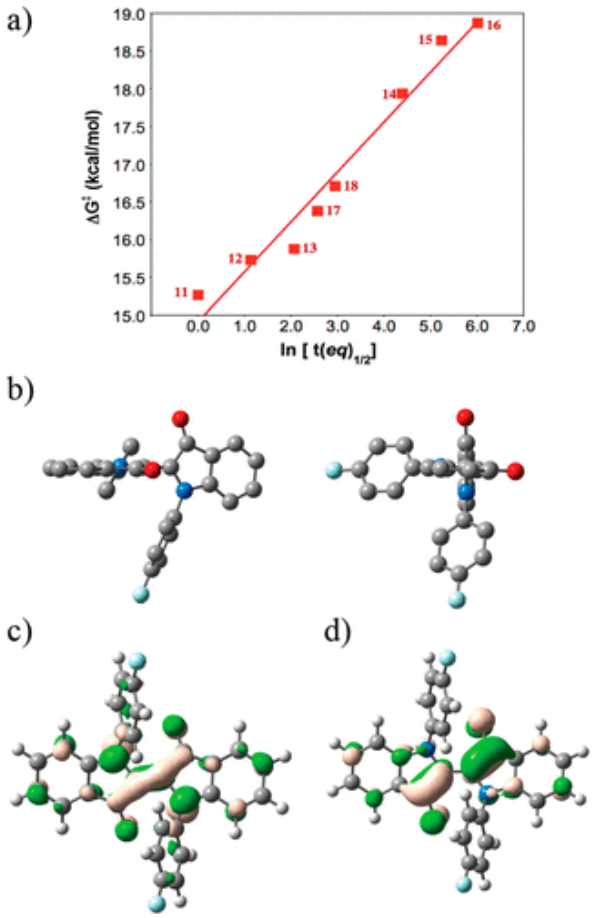

Figure 5. (a) Correlation between the experimentally determined ln(t(eq)$_{1/2}$) given in Table 4 and the PCM-(BS-)PBE0-D3^{BJ}/6-31G(d) computed free energy of the TS with respect to the *Z*-isomer ($\Delta G^{‡}$). (b) Two views of the TS obtained for **13** (H-atoms omitted for clarity). (c) HOMO of *E*-**13**. (d) LUMO of *E*-**13** (contour threshold: 0.04 au).